property of noble gases

	Density at 0℃,1atm (g/L)	Liquid Density (g/cm3)	Melting point(K)	Boiling point(K)
He	0.1786	0.145	-	4.22
Ne	0.9002	1.2	24.56	27.07
Ar	1.784	1.398	88.80	87.30
Kr	3.749	2.413	115.79	119.93
Xe	5.894 (2.7E19 atom/cm3)	3.053	161.4	165.03

Range of electron

$R_{ex}=542E-133$ ： $E>0.8MeV$

$R_{ex}=407E^{1.38}$ ： $0.15<E<0.8MeV$

Note: 出展忘れた。ガスでも正しいか要確認

Energy	Range (mg/cm2)	Range					
		gas at 1atm,0℃) (m)			Liquid (cm)		
		He	Ar	Xe	He	Ar	Xe
122 keV	22	1.23	0.12	0.04	0.15	0.02	0.01
662 keV	230	12.88	1.29	0.39	1.59	0.16	0.08
1.33 MeV	588	32.92	3.30	1.00	4.06	0.42	0.19
2.529 MeV	1240	69.43	6.95	2.10	8.55	0.89	0.41
3 MeV	1493	83.59	8.37	2.53	10.30	1.07	0.49

Table 5.1 Values of the Energy Dissipation per Ion Pair (the *W*-Value) for Different Gases[a]

Gas	First Ionization Potential (eV)	*W*-Value (eV/ion pair)	
		Fast Electrons	Alpha Particles
Ar	15.7	26.4	26.3
He	24.5	41.3	42.7
H_2	15.6	36.5	36.4
N_2	15.5	34.8	36.4
Air		33.8	35.1
O_2	12.5	30.8	32.2
CH_4	14.5	27.3	29.1

[a]Values for *W* from ICRU Report 31, "Average Energy Required to Produce an Ion Pair," International Commission on Radiation Units and Measurements, Washington, DC, 1979.

G.F.KNOLL, Radiation Detection and Measurement

A.O.Allen, Drift Mobilities and Conduction Band Energies of Excess Electrons in Dielectric Liquids

TABLE 1. Zero-field mobility of electrons (or negative ions) in condensed phases of elements and diatomic gases

Substance	State	μ_- $cm^2V^{-1}s^{-1}$	T, K	Temp. effect, equation	Temp. range, K
He	liq.	0.020	4.2	See fig. 1	0.274–5.18
Ne	solid	600.	25.	—	—
	liq.	0.0016	25.5	$\mu_- = 3.0 \times 10^{-4}T + 0.0070$	26–31
	liq.	0.0008	25.5	$\ln(\mu_- T) - 2.03 - (151/T)$	25.5–43
Ar	solid	1000	82	—	—
	liq.	475	85	—	—
	liq.	470	90.1	See fig. 2	90–160
Kr	solid	3700	113	—	—
	liq.	1800	117	—	—
	liq.	1300	120	See fig. 5	120–180
Xe	solid	4500	157	—	—
	liq.	2200	163	—	—
		1080	167	See fig. 6	167–315
N_2[a]	solid	0.0017	63	—	—
	liq.	0.00065	63	$\mu_- = 3.57 \times 10^{-5}T - 0.00160$	63–77
O_2[a]	liq.	0.00045	62	$\mu_- = 3.70 \times 10^{-5}T - 0.00185$	62–89
CO[a]	solid	0.003	68	—	—
	liq.	0.00087	69	$\mu_- = 4.78 \times 10^{-5}T - 0.00242$	69–78
H_2[a]	liq.	0.0086	21	—	—
Sulfur[a]	liq.	0.000100	393	$E_{activn.} = 0.15 \pm 0.02$ eV	393–433

[a]Interpretation of these data as electronic rather than ionic mobilities is quite doubtful; see text.

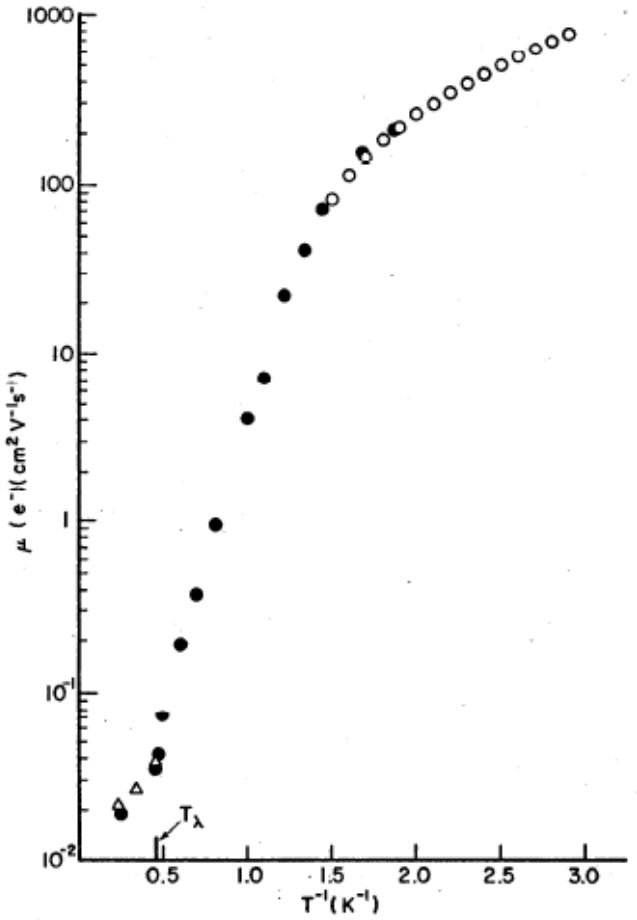

FIGURE 1. Mobility of electrons in liquid helium at pressures below 1 atm, plotted against recriprocal absolute temperature: open circles [729251]; closed circles [6000073]; open triangles [620159].

密度的には、液体ヘリウムが魅力的だが、液体Heでは、electronがドリフトしない！！！

- Ar(ガス)をSTPに対して40倍の密度で使うことを考える。
- Arを使うメリット: 無尽蔵に手に入る！
- Arを使うデメリット : バックグラウンドソースを含む。
- 3MeV電子の飛程が~210mmなので、10~30mm程度のsegmentationで読み出し、dE/dXを測る。
  - α粒子は、確実に落とせる。
  - γもかなり落とせる。
  - dE/dXでβを落とせるか？ (need study!!)
- Volumeを考えるとLiq. Arも魅力的。その場合は、trackingとは別の識別法が必要。(scintillation光？)。オプションとして、完全には捨てない。

Energy	Range (mg/cm2)	Range	
		gas at 1atm,0℃) (m)	Gas at 40 atm(0℃) (mm)
122 keV	22	0.12	3.1
662 keV	230	1.29	32.2
1.33 MeV	588	3.30	82.4
2.529 MeV	1240	6.95	173.8
3 MeV	1493	8.37	209.2

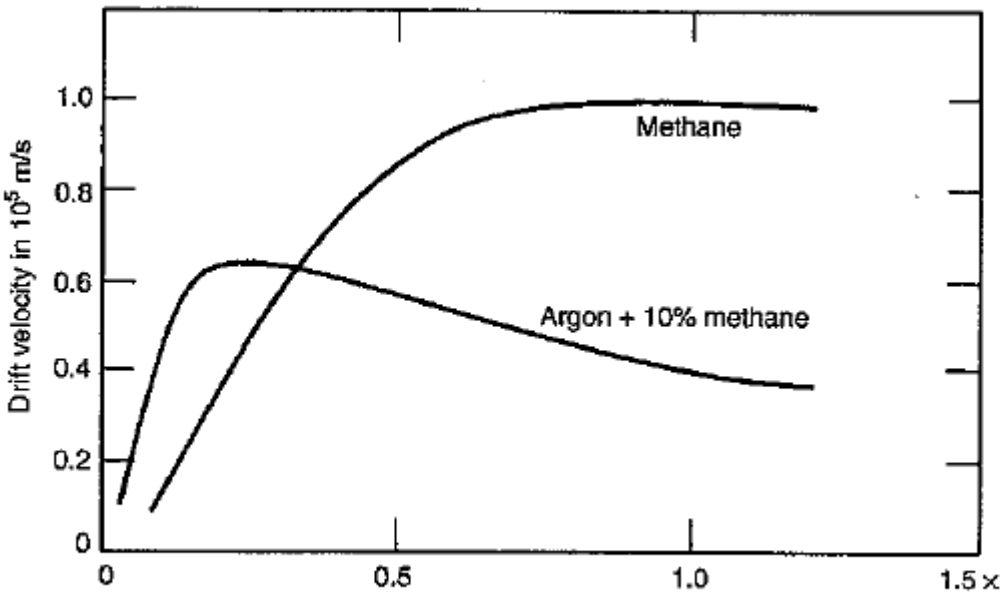

Figure 5.2 Electron drift velocity as a function of electric field $\mathscr{E}$ divided by gas pressure p. (Data

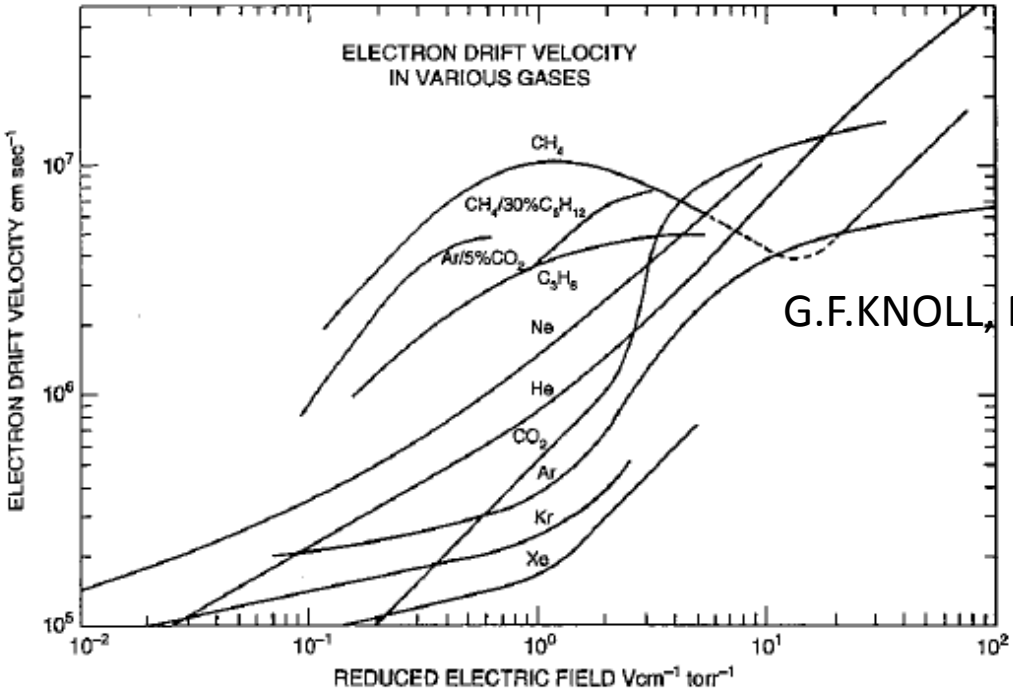

G.F.KNOLL, Radiation Detection and Measurement

Figure 6.17 The electron drift velocities in various gases, as compiled by Jeavons et al.[75]

C. The Gridded Ion Chamber

The dependence of the pulse amplitude on position of interaction in electron-sensitive ion chambers can be removed through the use of an arrangement sketched in Fig. 5.17. There the volume of the ion chamber is divided into two parts by a *Frisch grid*, named after the originator of the design.[27] Through the use of external collimation or preferential location of the radiation source, all the radiation interactions are confined to the volume between the grid and the cathode of the chamber. Positive ions simply drift from this volume to the cathode. The grid is maintained at an intermediate potential between the two electrodes and is made to be as transparent as possible to electrons. Electrons are therefore drawn initially from the interaction volume toward the grid. Because of the location of the load resistor in the circuit, neither the downward drift of the ions nor the upward drift of the electrons as far as the grid produces any measured signal voltage. However, once the electrons pass through the grid on their way to the anode, the grid–anode voltage begins to drop and a signal voltage begins to develop across the resistor. The same type of argument that led to Eq. (5.15) predicts that, for a circuit time constant large compared with the electron collection time, the time-dependent signal voltage across the resistor is

$$V_R = \frac{n_0 e}{dC} v^- t \tag{5.20}$$

where d is now the grid–anode spacing. This linear rise continues until the electrons reach the anode (see Fig. 5.17*b*). The maximum signal voltage is therefore

$$V_{\max} = \frac{n_0 e}{C} \tag{5.21}$$

G.F.KNOLL, Radiation Detection and Measurement
Chap. 5 Ionization Chambers

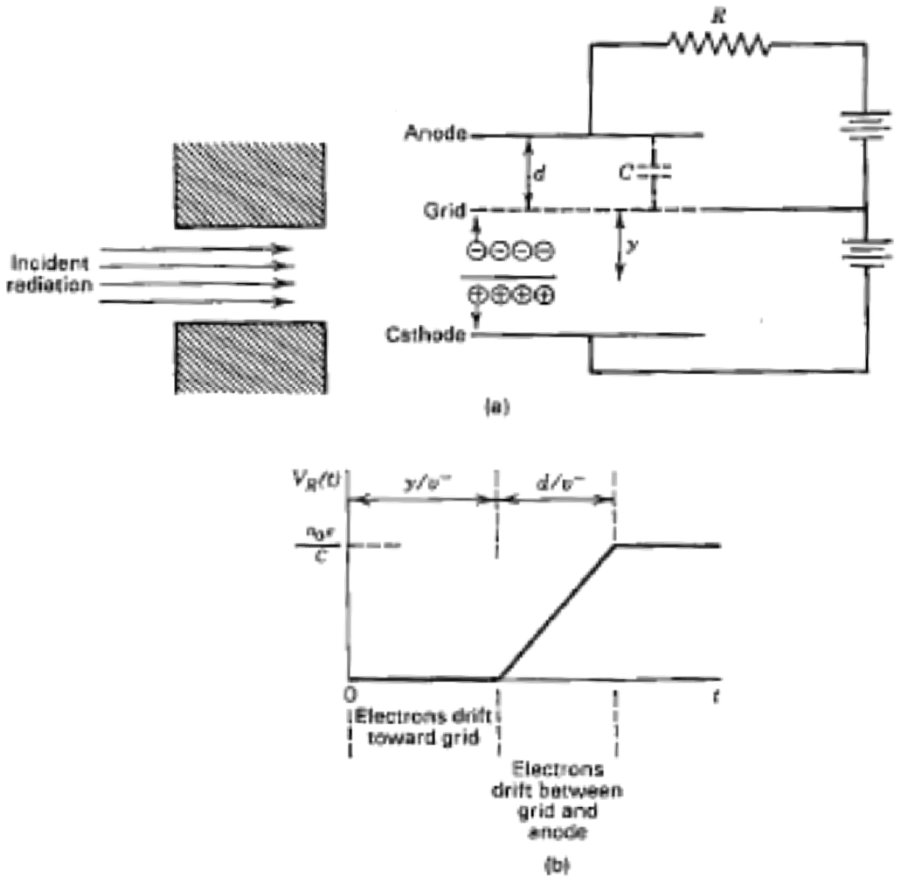

Figure 5.17 (*a*) Operational principle of the gridded ion chamber. All ion pairs must be formed in the lower region of the chamber between the cathode and grid. (*b*) The pulse shape that results from the formation of n_0 ion pairs at a distance y from the grid, where d is the grid–anode spacing [see part (*a*)]. The rise of the pulse results from the drift of the electrons across the grid–anode region. The pulse will decay back to zero with a time constant given by RC.

which is identical to Eq. (5.18). However, now the signal is derived only from the drift of electrons rather than from the motion of both electrons and positive ions. The slow rise corresponding to the drift of ions is eliminated, and the circuit time constant can therefore be set at a much shorter value typical of the electron-sensitive mode of operation described in the previous section. Since each electron passes through the same potential difference and contributes equally to the signal pulse, the pulse amplitude is now independent of the position of formation of the original ion pairs and is simply proportional to the total number of ion pairs formed along the track of the incident particle.

G.F.KNOLL, Radiation Detection and Measurement
Chap. 5 Ionization Chambers

Gridを通り過ぎた電子の誘起信号のみを見るので、放射線の発生位置やイオンの移動に無関係に最初に生成されたイオン対の数に比例した信号を観測できる。陽イオンのmobilityは3桁落ちなので、必須。

“Noble Gas Detectors”より

5.3
Triode Ionization Chamber

The single-carrier ionization chamber, requires that a grid electrode be placed in front of the anode to shield the electric field from ion charges, as illustrated in Fig. 5.10.

The potential of the grid electrode is generally kept constant. The leakage factor of the electric lines from the positive ions is given as the shielding inefficiency, η, as follows [272]:

$$\eta = \{s/(2\pi d_2)\}\log(1/\rho)$$
$$\rho = 2\pi r/s, \tag{5.12}$$

where d_2 is the distance from the grid to the anode, s is the spacing between adjacent wires, and r is the radius of the wire. If the chamber has a grid electrode, as described above, then the effect of positive ions is reduced to $\eta \times (Q_0/C_0)(X/d)$. For example, if $r = 0.005$ cm, $s = 0.1$ cm, $d = 3$ cm, and $\eta = 0.36\%$. Thus, even if the range of alpha particle R is equal to d, the width given for the diode is reduced to $\eta \times 0.6(Q_0/C_0)$.

The electrons produced by an alpha particle must pass through the grid without being captured by the grid. To do so, the electric lines must pass through the grid without interruption except for each center line of the wire as illustrated in Fig. 5.11, since electrons move along the electric lines. The

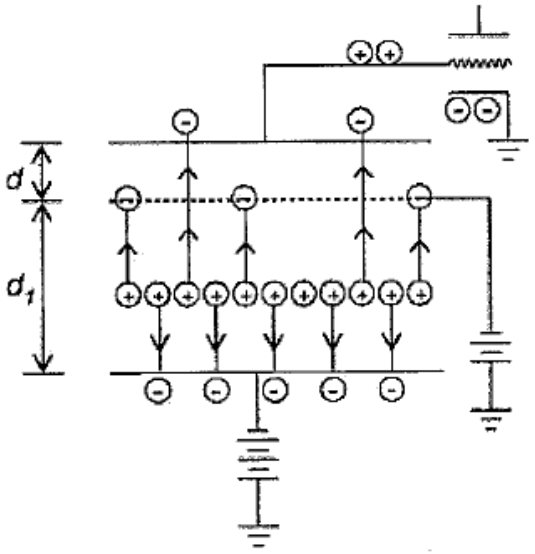

Fig. 5.10 Parallel plate gridded ionization chamber.

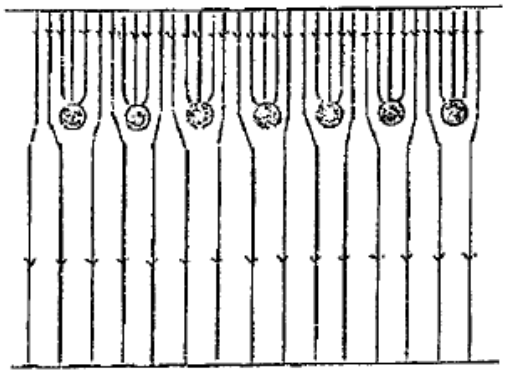

Fig. 5.11 Map of electric field lines in the vicinity of grid wires.

following formula is the condition for realizing the above pattern [272]:

$$Z > (1+\rho)/(1-\rho), \tag{5.13}$$

where Z is the ratio of the electric field between the anode and grid to that between the grid and cathode. This type of chamber is usually referred to as a gridded ionization chamber or a Frisch grid chamber.

E. Statistical Limit to Energy Resolution

The theoretical limit to the energy resolution set by the statistics of charge carrier formation in an ion chamber can be predicted from the discussion given in Chapter 4. As an example, let us assume that alpha particles with energy of 5.5 MeV are fully stopped in a gas with W-value of 30 eV/ion pair and a Fano factor of 0.15. As a first step, we can calculate the expected average number of ion pairs n_0 produced in the gas to be

$$n_0 = \frac{E_d}{W} = \frac{5.5 \times 10^6 \text{eV}}{30\,\text{eV/ion pair}} = 1.83 \times 10^5 \text{ ion pairs}$$

The variance in this number is given by

$$\sigma_{n_0}^2 = F n_0 = 0.15\left(1.83 \times 10^5\right) = 2.75 \times 10^4$$

The standard deviation, or the square root of the variance, is then

$$\sigma_{n_0} = \sqrt{F n_0} = \sqrt{2.75 \times 10^4} = 166$$

For the expected Gaussian distribution describing n_0, the full-width-at-half-maximum (FWHM) is just the shape factor of 2.35 multiplied by σ, leading to

$$\text{FWHM}(n_0) = 2.35\sigma_{n_0} = 390$$

Finally, since W units of energy are required to create one ion pair, the FWHM in units of particle energy is

$$\text{FWHM}(E) = 2.35\sigma_{n_0} \cdot W = 390(30\,\text{eV}) = 11.7\,\text{keV}$$

For ion chambers, this figure would conventionally be quoted as the energy resolution. Alternatively, the energy resolution could be quoted as a percentage by dividing the above figure by the deposited energy

$$R = \frac{2.35\sigma_{n_0} W}{E_d} = \frac{11.7 \times 10^3\,\text{eV}}{5.5 \times 10^6\,\text{eV}} = 0.213\%$$

This excellent energy resolution is almost never achieved in practice (see next page) because sources of electronic noise dominate over the statistical contributions.

G.F.KNOLL, Radiation Detection and Measurement
Chap. 5 Ionization Chambers

F. Charged Particle Spectroscopy

There are applications in which pulse-type ion chambers can be used to good advantage for the measurement of charged particle energies. Although it is much more common to use semiconductor detectors for this purpose (see Chapter 11), ion chambers offer features that may be attractive in some circumstances. They can be constructed with almost arbitrary size and geometry, and the gas pressure can be chosen to tailor the stopping power or effective thickness of the active volume. Ion chambers are also far less subject to performance degradation due to radiation damage than semiconductor detectors. Their design is generally quite simple, and they can be fabricated by many users with standard workshop facilities.

Pulse-type ion chambers have found application in a number of circumstances where their unrestricted size and other characteristics[27] have been exploited. They have proved useful in low-level alpha particle measurements[29,30] where parallel-plate-type gridded ion chambers have been constructed with cross-sectional areas up to 500 cm^2. Even larger chambers can conveniently be constructed by using cylindrical geometry. In order to achieve good energy resolution, a Frisch grid is normally incorporated into the chamber design. Because of the small amplitude of typical pulses, special care must be taken in choosing a low noise preamplifier and in minimizing mechanical vibrations, which, by modulating the detector capacitance, can give rise to interfering microphonic noise.[31] Using standard techniques, one can achieve energy resolution for 5 MeV alpha particles of 35–45 keV for such chambers.[29] By using a cooled preamplifier to reduce the electronic noise, suppressing vibrations, and operating under carefully-controlled laboratory conditions, an energy resolution has been demonstrated[32] of 11.5 keV for alpha particles. This energy resolution is essentially at the limit set by charge carrier statistics and is comparable to the best that currently can be achieved using silicon semiconductor detectors.

11.5 keV/ 5MeV = 0.23%!

28. H. W. Fulbright, *Nucl. Instru. Meth.* **162**, 21 (1979).
29. H. Hoetzl and R. Winkler, *Nucl. Instrum. Meth.* **223**, 290 (1984).
30. C. W. Sill, *Health Phys.* **69**(1), 21 (1995).
31. G. F. Nowack, *Nucl. Instrum. Meth.* **A255**, 217 (1987).
32. G. Bertolini, *Nucl. Instrum. Meth.* **223**, 285 (1984).

G.F.KNOLL, Radiation Detection and Measurement
Chap. 5 Ionization Chambers

Proportional counter

C. Fill Gases

The noble gases, either pure or in binary mixtures, can be useful proportional gases provided the gas multiplication factor is kept below about 100.[12] Beyond this point, adding a quench gas is helpful[13,14] in reducing instabilities and proportionality loss caused by propagation of ultraviolet photons. Because of cost factors, argon is the most widely used of the inert gases, and a mixture of 90% argon and 10% methane, known as *P–10 gas*, is probably the most common general-purpose proportional gas. When applications require high efficiency for the detection of gamma-ray photons by absorption within the gas, the heavier inert gases (krypton or xenon) are sometimes substituted. Many hydrocarbon gases such as methane, ethylene, and so on are also suitable proportional gases and are widely applied where stopping power is not a major consideration. In applications where the signal is used for coincidence or fast timing purposes, gases with high electron drift velocities are preferred (see Fig. 6.17 later in this chapter). Proportional counters used for thermal neutron detection are operated with BF_3 or

G.F.KNOLL, Radiation Detection and Measurement
Chap. 6 Proportional Counters

The basic properties of a fill gas can be changed significantly by small concentrations of a second gas whose ionization potential is less than that of the principal component. One mechanism, known as the *Penning effect*, is related to the existence of long-lived or metastable excited states in the principal gas. If the excitation energy is larger than the ionization energy of the added component, then a collision between the metastable excited atom and a neutral additive atom can ionize the additive. Because the excitation energy would otherwise be lost without the additive, a greater number of ion pairs will be formed per unit energy lost by the incident radiation. For example the *W*-value for argon can be reduced from 26.2 to 20.3 eV through the addition of a small concentration of ethylene.[22] Furthermore, because a greater fraction of the incident radiation energy is converted into ions, the relative fluctuation in the total number of ions is decreased by as much as a factor of two.[22] Because of the corresponding improvement in energy resolution, fill gases that consist of Penning mixtures are commonly chosen for proportional counters applied in radiation spectroscopy.[23–28] Some values for *W* and the Fano factor *F* for common proportional gases are given in Table 6.2 later in this chapter. Other values measured for noble gases and their mixtures are reviewed and reported in Refs. 29–32. It should be emphasized that these parameters are not to be regarded as universal constants but that some mild dependence of *W* and *F* on particle type and/or energy is experimentally observed. The energy dependence is often most evident for X-rays and gamma

Penning効果によって、W値やFano係数が改善する。
次ページ参照

G.F.KNOLL, Radiation Detection and Measurement
Chap. 6 Proportional Counters

$$\frac{\sigma_Q}{Q} = \sqrt{\frac{F+b}{n_0}}$$

@3 MeV, FWHM

Ar

Ionization only → 0.29%

Proportional mode → 0.57%

Ar+0.5%C_2H_2

Ionization only → 0.14% !

Proportional mode → 0.42%

Table 6.2 Resolution-Related Constants for Proportional Gases

Gas	W (eV/ion pair)	Fano Factor F Calculated[a]	Fano Factor F Measured	Multiplication Variance b	Energy Resolution at 5.9 keV Calculated[b]	Energy Resolution at 5.9 keV Measured
Ne	36.2	0.17		0.45	14.5%	
Ar	26.2	0.17		0.50	12.8%	
Xe	21.5		≤ 0.17			
Ne + 0.5% Ar	25.3	0.05		0.38	10.1%	11.6%
Ar + 0.5% C_2H_2	20.3	0.075	≤ 0.09	0.43	9.8%	12.2%
Ar + 0.8% CH_4	26.0	0.17	≤ 0.19			
Ar + 10% CH_4	26[c]			0.50	12.8%	13.2%

[a]From Alkhazov et al.[22]

[b]Given by $2.35[W(F+b)/5900\ \text{eV}]^{1/2}$ [see Eq. (6.24)].

[c]From Wolff.[52]

Source: Adapted from Sipila.[59]

G.F.KNOLL, Radiation Detection and Measurement
Chap. 6 Proportional Counters

Proportional領域では、環境要因で増幅度が大きく変化

Table 6.3 Gain (Pulse Height) Variations in a Proportional Counter

Predictions of the Diethorn model for a P-10 filled proportional tube, $a = 0.003$ cm, $b = 1$ cm, $V = 1793$ V, $M = 1000$:

1% increase in	Change in M:
Applied voltage V	+17.4%
Gas pressure p	−8.6%
Anode radius a	−6.1%
Cathode radius b	−2.7%

G.F.KNOLL, Radiation Detection and Measurement
Chap. 6 Proportional Counters

Micro Patter Gas detectors

e.g. Mircromegs

By proper choice of the applied voltages, most of the positive ions produced in the avalanches are collected by the mesh. Minimizing the distance over which they must drift promotes rapid recovery from space charge effects and permits operation at high rates. This small gap is normally accomplished by the use of insulating pillars or other supports between the mesh and anode planes. Inevitable small dimensional variations in the gap thickness do not strongly affect the avalanche size, since a smaller gas thickness is compensated by a higher electric field in that local region. If the anode consists of a position-sensitive configuration such as strips or pixels, then the centroid of the avalanches that are formed can be spatially recorded. The spatial resolution can be as good as 10 to 15 microns under favorable circumstances.[156]

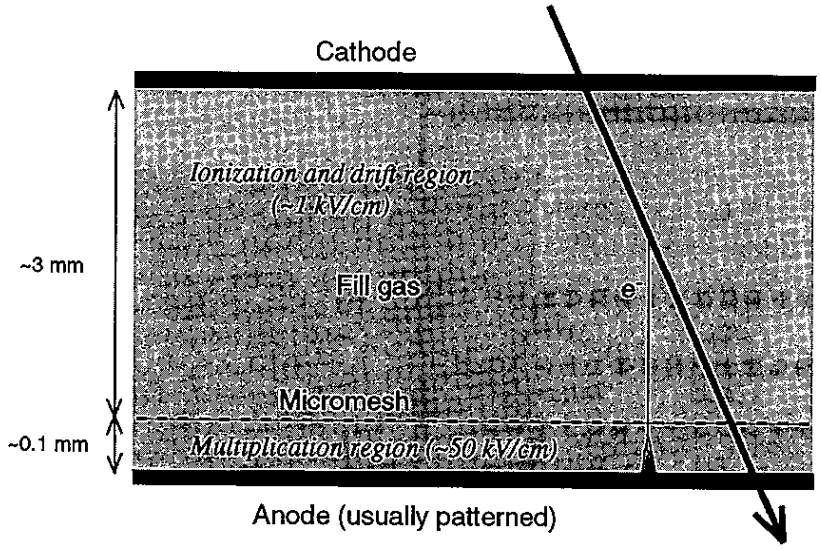

Figure 6.31 Basic principle of a Micromegas detector. Ionization electrons formed in the upper portion of the gas-filled chamber drift downward in a moderate electric field and pass through the micromesh into the multiplication region. There the electric field strength is much higher, and avalanches form.

Because each avalanche is approximately the same size, the amplitude of the pulse produced at the anode is proportional to the number of ion pairs formed in the ionization region of the chamber. For soft radiations such as low-energy X-rays, the thickness of a few millimeters of typical fill gases is sufficient to fully absorb the incident energy in at least some fraction of the cases. Thus X-ray energy spectra can be recorded, and values of energy resolution have been measured[157,158] for 5.9 keV X-rays that are about 12% FWHM, nearly the same as observed from conventional proportional tubes (see Table 6.2).

While most applications have been in high-energy particle tracking, there has

Gas Proportional Scintillation Counters

G.F.KNOLL, Radiation Detection and Measurement
Chap. 6 Proportional Counters

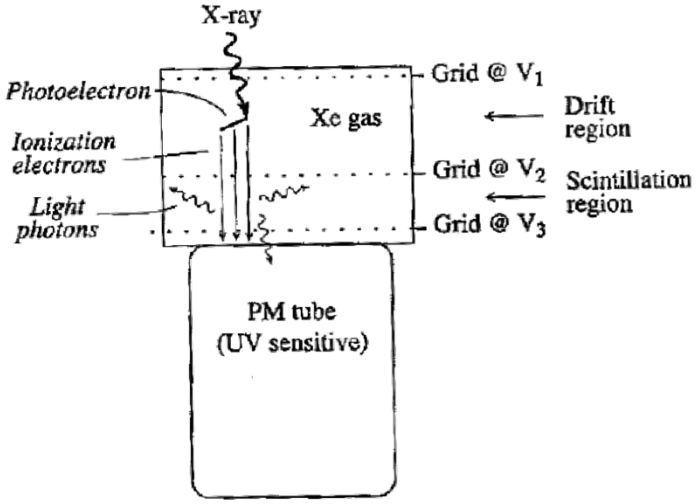

Figure 6.24 Schematic of a gas proportional scintillation counter with a low-field drift region and a higher-field scintillation region. All the light is generated in the scintillation region.

Table 6.4 Spectral Properties of Light Emitted in Gas Proportional Scintillation Counters

Gas	Peak Wavelength of Emission Spectrum (nm)	FWHM of Emission Spectrum (nm)
Argon	128	10
Krypton	147	12
Xenon	173	14

Data from Suzuki and Kubota.[138]

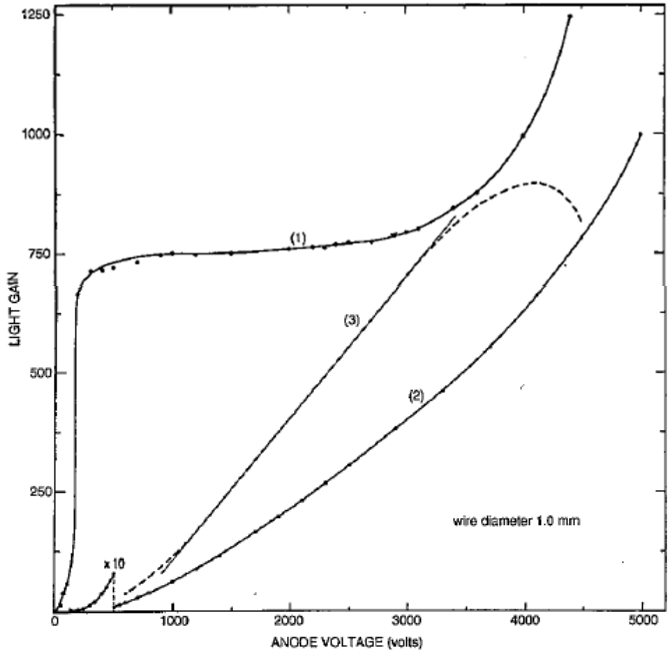

Figure 6.25 Curves showing the relative charge gain (1), light gain (2), and secondary light per collected electron (3), for a gas proportional scintillation counter. A numerical scale is shown for curve (2) only. Charge multiplication begins at about 3 kV, but secondary light production is observed at much lower anode voltages. (From Policarpo et al.[143])

Ionizationの増幅よりもかなり先に(弱い電場で)、scintillation光増幅が起きる。

Ionization v.s. Proportional

- ✓ Ionization
  - Ultimate resolution
  - Signal is very small $\rightarrow$ Need fancy (and cooled) preamp
  - Simple electrode
- ✓ Proportional
  - x100 to keep energy resolution $\rightarrow$ normal preamp for semiconductor
  - Wire or micropattern gas detector
  - strong dependence of multiplication factor on environment(gas pressure, HV, wire) $\rightarrow$ bad influence on energy resolution

KNOLLより

Preampについて(1)

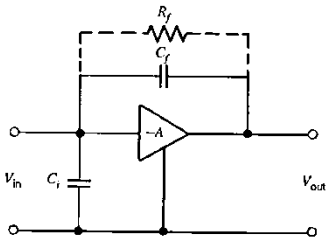

Assume $A >> (C_i + C_f)/C_f$

$V_{out} = -A\ V_{in}$

$V_{out} = -A \dfrac{Q}{C_i + (A+1)C_f}$

$V_{out} \cong -\dfrac{Q}{C_f}$

Figure 16.13 Simplified diagram of a charge-sensitive preamplifier configuration. If the conditions indicated are met, the output pulse amplitude becomes independent of the input capacitance C_i. The time constant given by the product R_fC_f determines the decay rate of the tail of the output pulse.

3. NOISE CHARACTERISTICS

Probably the most important specification for a preamplifier is its noise figure. This specification is normally quoted as the FWHM of the response function of the system that is due only to the preamplifier noise. The figure is normally given as the equivalent energy spread in the type of detector for which the preamplifier is designed. The noise figure is a strong function of the capacitance with which the preamp input is loaded. For example, a good-quality preamplifier used with silicon diode detectors may have a noise figure of 1.6 keV with zero input capacitance, but this figure may double if the input is loaded with 100 pF. The input capacitance arises from both the inherent detector capacitance and from the connecting cable between the detector and preamplifier. It is therefore important to keep the interconnecting cable as short as possible and to choose a detector whose inherent capacitance is no larger than necessary.

One of the significant contributors to preamplifier noise is the Johnson noise associated with the feedback resistor (R_f in Fig. 16.13). The noise is made smaller by increasing the resistance value, but the longer time constant leads to very long tails on the output pulses. Problems can then arise with respect to overload recovery and pile-up in the preamplifier (see below). An alternative approach is to eliminate the feedback resistor altogether. Two preamplifier designs that do not require resistive feedback are called *pulsed optical feedback* and *transistor reset* preamplifiers. Their operation is described beginning on p. 618. In both cases, the elimination of the feedback resistor and its Johnson noise permits a lower preamplifier noise contribution compared with conventional resistive feedback preamplifiers.

In demanding situations, the noise generated in the preamplifier input stage can also be reduced by cooling. The practical problems involved generally make this approach unattractive except in the case of applications in which the detector itself is operated at reduced temperature. Most cooled preamplifier applications are therefore in conjunction with germanium or Si(Li) detectors, for which the first stage of the preamp is held near liquid nitrogen temperature inside the detector cryostat, or with semiconductor X-ray detectors that are used with Peltier electrical cooling.

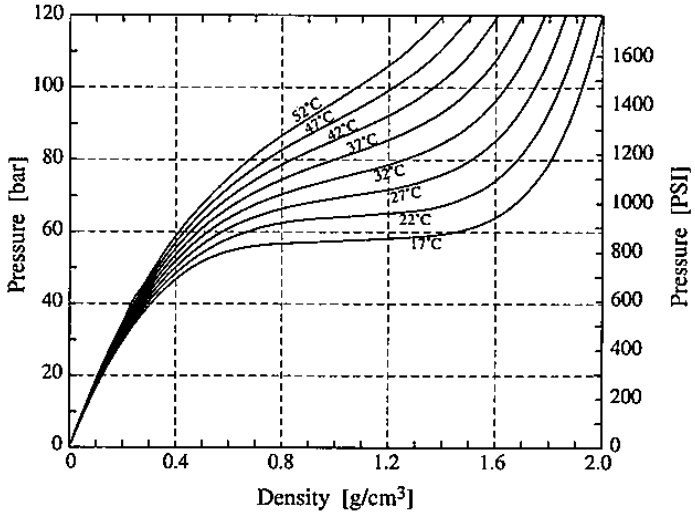

Figure 19.5 Relationship of density and pressure of xenon at the constant temperatures shown. (From Mahler et al.[22])

KNOLLより

Xenon gas at pressures near its critical point (58 atm, 17°C, density of 1.1 g/cm^3) represents an attractive medium for gamma-ray spectroscopy. The high atomic number (54) of xenon promotes the photoelectric absorption process that is important for full conversion of the incident gamma-ray energy to charge. Gaseous detectors are not limited to small volumes by constraints of crystal growth or other fabrication considerations. While there have been some examples of the use of high-pressure xenon in proportional counters[18] or proportional scintillation detectors,[19] principal interest has been in its use in pulse mode ion chambers.[20,21] Because of the short mean free path of electrons in the high-density gas, typical drift velocities are limited to around 10^5 cm/s for reasonable electric field values. It has been demonstrated[22] that for a density of 0.5 g/cm^3, the free electron lifetime is about 5 ms for an electric field of 2×10^5 V/m, sufficiently long to allow over 99% charge collection efficiency in chambers of typical dimensions. Achieving this long lifetime, however, requires the strictest attention to eliminating impurities that might attach free electrons. Chambers must be constructed using ultrahigh vacuum techniques to avoid the inclusion of any organic materials, and electronegative impurities must be maintained below about 0.5 ppm.

Xenon at high pressures is far from an ideal gas and has a very high compressibility near its critical point, as illustrated in Fig. 19.5. For example, at a density of 0.8 g/cm^3, the pressure will increase from 56 to 88 atmospheres with a temperature change from 17 to 52°C. Provided that the pressure boundary is designed to sustain these high pressures, xenon chambers have the added virtue of being usable over wide temperature ranges without significant deterioration in their performance.[23,24] The chamber wall must be several millimeters thick in order to safely contain the pressurized gas. Using typical materials such as titanium or stainless steel, there will be severe attenuation of low-energy incident gamma-ray photons below about 100 keV.

Most successful demonstrations of the use of high-pressure xenon as a spectrometer medium[22,25] have used ion chambers fitted with a Frisch grid (see Chapter 5). The *W*-value of xenon at low pressure is 21.9 eV per ion pair. This value is observed to decrease gradually with increasing xenon density, and it is lower by about 15% when a density of 1.7 g/cm^3 is reached.[25] Using a Fano factor of 0.13, the energy resolution limit set by charge carrier statistics is about 0.5% at 662 keV. In practice, typical high-pressure gridded ion chambers show much poorer energy resolutions of 2–4%. The difference represents the added contributions of electronic noise and microphonics because of the very low-level signals that are produced. Relatively long shaping times must be used in processing electronics because of the slow drift velocity of the electrons, allowing more of the microphonic signal to affect the chamber resolution. To help speed the electron drift, it has been found that the addition of about 1% of hydrogen gas to the xenon enhances the drift velocity and promotes a faster output signal.[26]

Xenon also is a scintillator, and there will be prompt scintillation light emitted when the incident particle interacts in the gas. This light is in the ultraviolet region of the spectrum centered around 170 nm, and appears with a mixture of decay times of 2.2 and 27 ns. The appearance of this scintillation light can provide a "time zero" signal if the light can be conducted to an ultraviolet-sensitive photomultiplier tube outside the pressure boundary.[27] By timing the difference of the appearance of the scintillation light and the collection of the electrons at the anode, the drift distance can be deduced yielding the depth of the particle interaction within the gas.

IV. LIQUID IONIZATION AND PROPORTIONAL COUNTERS

similar to conventional ionization or proportional counters. A comprehensive review of noble gas detectors is included in the book published as Ref. 29.

Some properties of liquified noble gases of interest in detector applications are given in Table 19.1. Of these, liquid xenon has received the most attention and has been applied successfully both as a conventional ion chamber, where the charges are simply collected, and as a proportional counter, in which charge multiplication occurs at high values of the electric field. The electron drift velocity saturates at 3×10^3 m/s for electric field values greater than about 10^5 V/m (Refs. 30 and 31). The onset of multiplication is observed to occur at about 10^8 V/m (Ref. 32).

KNOLLより

Table 19.1 Properties of Some Condensed Media for Ionization Chambers

	Z	$\left(\frac{g}{cm^3}\right)$	Boiling Point	W (eV/ion pair)		F (Fano factor)	
				Calculated[a]	Experimental[a]	Model 1[b]	Model 2[c]
Liquid Ar	18	1.41	87 K	23.3	23.6	0.107	0.116
Liquid Kr	36	2.15	120 K	19.5		0.057	0.070
Liquid Xe	54	3.52	166 K	15.4	15.6	0.041	0.059
			Melting point				
Solid Ar	18	1.62	84 K				

[a]From T. Doke et al.[28]

[b]Based on W. Shockley, *Czech. J. Phys.* **B11**, 81 (1961).

[c]Based on G. D. Alkhazov et al., *Nucl. Instrum. Meth.* **48**, 1 (1967).

If the impurity concentrations are kept very low (less than one part per billion of oxygen equivalent), the distance over which electrons can be drifted in liquid argon or xenon approaches a meter or more.[33] Chambers with large active volume are therefore feasible, and position-sensing can be carried out by measuring the electron drift time.[34] The energy resolution in small gridded ionization chambers is typically 5–6% for gamma rays,[35] but values of 2.7% in liquid argon[36] and 4.3% in liquid xenon[37] have been reported for 976 keV conversion electrons. These figures are still much poorer than predicted from theory, and it is thought that the degradation in resolution is caused by variations in recombination that is due to a high density of ions and electrons along the tracks of delta rays (low-energy electrons) produced in large numbers along the primary path.[38–40] An ultraviolet photon is often emitted in the recombination process, and efforts have been made to "reclaim" the lost ionization by mixing an organic dopant with low photoionization threshold into the liquid. There have been some reported results[37] that indicate an improved energy resolution with this approach.

Liquid argon is also a scintillator, as described in Chapter 8. Most of the scintillation light derives from excited molecules that are formed by the recombination of ion–electron pairs. Applying an electric field near 10^6 V/m to collect the free electrons also suppresses recombination, and the scintillation intensity drops to one-third of its zero field value. Both scintillation and ion chamber signals can be measured simultaneously from the same sample of liquid argon,[41] and it is observed that the sum of the two signals is approximately independent of electric field strength.

It is also possible[42,43] to operate liquid xenon chambers in the proportional-scintillation mode (see p. 193). This choice has the potential advantage of more stable operation than one in which charge multiplication is required. Again, both the scintillation light and the collected charge can serve as independent measures of the energy deposition. This approach also lends itself to applications in which sensing the position of interaction is important.[44] A number of strategies have evolved that incorporate charge and/or light collection from liquid xenon that lead to measurement of both energy deposition and position of interaction in volumetric detectors. These advanced instruments have demonstrated useful characteristics for applications in the imaging of gamma rays in astrophysics[45,46] and in medical imaging.[47,48]

Some attention has been given to solid rather than liquid argon.[49] The electron mobility is actually higher in the solid phase,[30] but problems related to poisoning and polarization of the solid have inhibited further development.

A unique detection scheme involves generating charges in the liquid phase of a condensed gas, and then extracting the ionization electrons into a vapor phase of the same gas. These "two-phase electron emission devices" exploit the high interaction probabilities afforded by the high density of the liquid, together with the ease of multiplying the charge or generating light when the electrons are accelerated by an electric field in the gas phase. They provide interesting capabilities [50,51] in applications that involve detection of small signals that might not be directly observable above noise in the liquid phase.